A Protocol Using Compact 3D Printed Micro-Optical Elements for Protein Identification from Low-Intensity Amino-Acid Raman Signals

Jannis Weinacker,* Bikash Kumar Bhandari, Alba Viejo Rodriguez, Charlotte West, Francesco De Angelis, Francesco Tantussi, Nicolò Maccaferri, Nick Goldman, and Martin Wegener*

When performing optical high-speed single-molecule spectroscopy and identification, low signal intensities pose a challenge. Fortunately, for many applications, the number of possible molecules in the specimen is small or limited. For such cases, a protocol is presented that uses only a small number of very sensitive hence expensive detectors. The protocol starts with optimizing spectral regions, one per detector, so that different molecules become best distinguishable. Experimentally, the spectral regions are extracted from the continuous spectrum using a custom-made micro-optical element. In the ray-optics picture, it guides all rays in a spectral region onto the entrance of an optical fiber connected to one detector. The shape of the micro-optical element is derived by applying Snell's law to the given geometrical boundary conditions. A proof-of-concept measurement using a dedicated demonstrator refractive optical element in combination with a continuous white-light source is performed. Indeed, the element selects the correct spectral regions and couples the light into the correct fibers. For the example of the identification of single amino acids in a protein, the protocol leads to a higher correct identification rate. Therefore, this protocol is useful for such protein identification experiments as performed in the EU project ProID.

1. Introduction

The identification or sensing of molecules with different spectroscopy techniques is widely spread in many medical applications,[1,2] biology,[3–5] and chemistry.[6,7] Due to their minimally invasive effects, Raman spectroscopy is an outstanding example.[8–11] Raman spectra carry on a large amount of information regarding molecular structure and composition often providing a fingerprint to identify molecules. Examples are single bases in DNA[12–15] and single amino-acids in proteins.[16–19]

The disadvantage of Raman is the weak signal that forces longer acquisition time with respect to methods based, for example, on fluorescence. Currently, nano optical approaches combined with plasmonic enhancement are pushing Raman analyses toward faster time scales. However, to reach millisecond or even

J. Weinacker, M. Wegener
Institute of Applied Physics (APH)
Karlsruhe Institute of Technology (KIT)
Wolfgang-Gaede-Str. 1, 76131 Karlsruhe, Germany
E-mail: jannis.weinacker@kit.edu; martin.wegener@kit.edu

J. Weinacker, M. Wegener
3DMM2O-Cluster of Excellence
Karlsruhe Institute of Technology (KIT) and Heidelberg University
76128 Karlsruhe, Germany

B. K. Bhandari, C. West, N. Goldman
European Molecular Biology Laboratory
European Bioinformatics Institute (EMBL-EBI),
Wellcome Genome Campus
Hinxton, CB10 1SD Cambridge, UK

ⓘ The ORCID identification number(s) for the author(s) of this article can be found under https://doi.org/10.1002/admt.202401876

A. Viejo Rodriguez, N. Maccaferri
Department of Physics
Umeå University
Linnaeus väg 24, Umeå 901 87, Sweden

A. Viejo Rodriguez, N. Maccaferri
Department of Physics and Materials Science
University of Luxembourg
162a avenue de la Faïencerie, Luxembourg 1511, Luxembourg

F. De Angelis, F. Tantussi
Plasmon Nanotechnology
Istituto Italiano di Tecnologia (IIT)
Via Morego 30, Genova 16163, Italy

M. Wegener
Institute of Nanotechnology (INT)
Karlsruhe Institute of Technology (KIT)
P.O. Box 3640, 76021 Karlsruhe, Germany

See the Terms and Conditions

**ADVANCED
SCIENCE NEWS**

www.advancedsciencenews.com

**ADVANCED
MATERIALS
TECHNOLOGIES**

www.advmattechnol.de

microsecond time scale is still extremely challenging. In this regard, the use of single photon detectors, such as SPAD, looks an interesting opportunity with respect to CMOS and CCD cameras usually adopted in Raman Spectrometers. Unfortunately, SPAD cameras providing high spectral resolution (large number of pixels tightly packed) are still very expensive. In this regard, the possibility of using few spectral points would be a clear advantage in terms of cost, volume, and even performances in case of fast measurements (SPAD detectors). In contrast, regardless the time scale of the measurement and the detector employed, questions arise on the number of pixels necessary to discriminate the molecule of interest or an entire class of molecules. In fact, current protocols for data analysis are advancing very fast due to the recent developments in the field of Machine Learning. This is also impacting on the analyses of Raman datasets. For instance, let's consider the 20 proteogenic amino acids which are the building blocks of proteins. Standard Raman spectrometers usually record up to 128 spectral points and this is known to be enough to distinguish all the amino acids. However, it is questionable how many points are really necessary to successfully discriminate aminoacids or what the most informative spectral regions are. In other words, considering that the spectra of amino acids are already well established, even at single molecule level, we wonder what is the minimum number of spectral points or spectral bands that are really needed. Also, what is their spectral position and bandwidth.

In this work, we show that few spectral bands, on the order of four, carry on enough information to identify the amino acids with a rate that allows a later identification of the protein with a high probability.[20] The four spectral regions are optimized such that the discrimination among the amino acids may be maximized. We also propose an experimental optical scheme optimized to record Raman spectra from a limited number of spectral bands.

For the possible experimental realization of our protocol, a way would be needed to guide the photons in the above-mentioned spectral regions to the corresponding detectors. For this purpose, we suggest a segmented refractive-optical element (SROE), for which we present its targeted functions and design protocol. In essence, this element consists of four focusing elements covering exactly the width of the corresponding spectral region in the spectrometer and focusing the light onto the entrance of one optical fiber each. Each fiber is then connected to a detector which can be of an almost arbitrary size. For demonstration, we fabricated an SROE with the commercially available 3D laser nanoprinter by Nanoscribe called QuantumX using two-photon grayscale lithography.[21] This technique allows to print transparent polymer structures with a surface-precision on the order of 100 nm[22] and optical-grade surface roughness.[23,24] We demonstrate the capabilities of the demonstrator SROE in a practical test using a white-light source and a custom-made spectrometer. By these experiments, we emulate actual Raman experiments on amino acids and couple the light from the four spectral regions into four optical fibers. By analyzing the spectra of the light coming out from the other ends of the four fibers, we find that the spectra indeed match the designed spectral regions.

2. Theoretical Section

2.1. Analytical Definition of the Four Spectral Regions

The goal of optimizing the spectral regions is to maximize the amount of information that can be used to faithfully decode the originating amino-acid. To do this, we first developed a way to quantify the useful information received by the detectors on the given spectral regions. In our case, we have four detectors D_i ($i = 1, \ldots, 4$), each of them spanning different intervals I_i ($i = 1, \ldots, 4$) in the wavenumber range and only able to detect photons in this range. The detector intervals are assumed to be non-overlapping.

For the wavenumbers ν and corresponding intensities $f^X(\nu)$ of Raman scattered photons from amino-acid X, we normalize $f^X(\nu)$ by the total intensity of Serine, where total intensity is the integral of $f^X(\nu)$ over the whole range of ν.[16,25] We used Serine because it has the highest total intensity in comparison to the other amino-acids. Therefore, the normalized total intensity will be one for Serine and less than one for the remaining amino-acids, and the average numbers of photons emitted (T) will now be relative to Serine. The relative photon detection rates of the detectors D_i ($i = 1, \ldots, 4$), denoted by r_i^X, is the sum of normalized intensities within the spectral regions of each detector. Our problem is to choose the four spectral regions such that the captured photons are maximally informative about the originating amino-acid.

Using Bayes theorem, the conditional posterior probabilities of inferring amino-acid Y from photons emitted from the true amino-acid X can be written as:

$$P(Y|X) \approx \text{prior}(Y) \times l_Y^X \tag{1}$$

Here, prior(Y) represents the prior belief on probable amino-acids, which we set to 1/20 for all amino-acids to represent an absence of any prior expectation about the origin of the photons. l_Y^X is the likelihood of observed data from amino-acid X conditional on inferred amino-acid Y. Assuming the emissions/detections are Poisson processes, the Poisson parameter μ_i for detector D_i is equal to the detection rate times the average number of photons received:

$$\mu_i^X = T\, r_i^X \tag{2}$$

In practice, T for a fast translocating molecule in an ultrafast Raman spectroscopy setup will likely be less than 100. Therefore, in this work, we study the cases of $T = 50$ and 100. The likelihood is then given by:

$$l_Y^X = \prod_{i=1}^{4} \frac{\left(\mu_i^Y\right)^{c_i^X} e^{-\mu_i^Y}}{c_i^X!} \tag{3}$$

where c_i^X are the photon counts from amino-acid X at detector D_i.

The mean of the diagonal elements of the confusion matrix $P(X|X)$ gives the expected probability of correctly inferring the true amino acid, a statistic which we name $M1$, so

$$M1 = \frac{1}{20} \cdot \sum_X P(X|X) \tag{4}$$
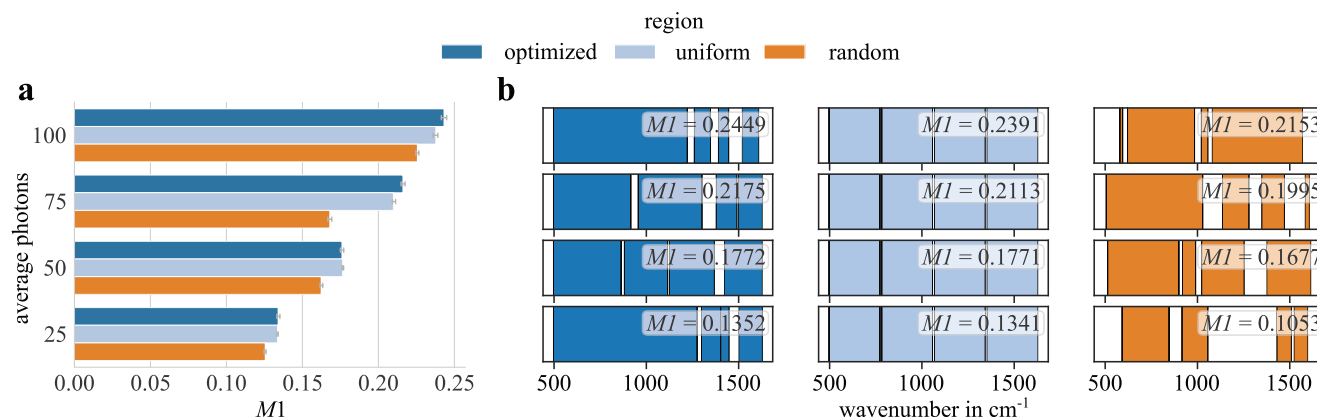
2401876 (2 of 7)

Figure 1. a) Comparison of M1 for different spectral regions and b) optimized regions with the maximum M1 out of all optimized regions. Optimized regions were obtained after maximizing M1. As controls, we also use randomly selected regions intervals, which are still not allowed to overlap, and uniformly separated regions with gaps of the size of 10 cm^{-1} which corresponds to the resolution limit of the presented imaging system (see Section 3.2 Testing the SROE). For optimized and random regions, we computed the bands ten times and evaluated M1. The regions were constrained between the wavenumbers 497 and 1628 cm^{-1}. The mean of ten M1 values for the bands on (b) is shown for each bar (a). Error bars represent the 100 % percentile interval. M1 increases with the average number of photons, indicating that the amino acid discrimination improves with the number of photons: indeed, randomly selected regions perform better with 100 photons than optimized regions for 50 photons. Nevertheless, it is evident that for a fixed photon number, optimized regions give slightly higher performance than random or uniformly spaced regions. b) The regions for each case with the highest M1 together with their M1 values are shown in the right subplots. The best optimized region shown is then used in this study (See Figure 3c,d) since they describe the most general case.

$M1$ runs from 0 to 1, indicating from no ($M1 = 0$) to perfect ($M1 = 1$) identification of amino acids, where $M1 = 0.05$ would be the no skill case for random guessing. Similarly, $M1$ of 0.243 (see **Figure 1**) means, on average, the probability of correctly inferring an amino acid using the given detector configuration is 0.243. Therefore, $M1$ reflects the discriminative power of the detectors subjected to some spectral regions. Using $M1$ as the cost function, optimization algorithms can then be used to optimize the spectral regions I_i (Figure 1). The performance of the optimized spectral regions is only 2.4% better than the performance of the uniform distribution with small gaps of 10 cm^{-1}. Nevertheless, we choose the optimized solution because the case of non-evenly spaced spectral regions with different widths represent a more general case, which is more demanding for the manufacturing of the laser-printed refractive optical element. For different scenarios, e.g., by using only a subset of amino acids for the optimization (see Supporting Information Section S6) a larger improvement of 8.9%, so almost 4 times as much, is achievable. The value of $M1$ after optimization depends on the average number of detected photons emitted by one amino acid as well as the number of detectors available. For the case of 50–100 photons on average, a higher number of detectors does not significantly improve the value of $M1$. Thus, a small number of four detectors is chosen in this study (see Section S5). From a computational point of view, it is more convenient to work with the log of the likelihood (see Supporting Information). The resulting form can be vectorized using the python library NumPy (v 1.22.3). Due to the stochastic nature of Poisson process, and thus $M1$, the standard optimization algorithms may be prone to returning suboptimal results. Therefore, we used gp_minimize, a Bayesian optimization algorithm, from scikit-optimize (v 0.9.0) to optimize $M1$. The full confusion matrix for the optimized spectral regions for 100 photons emitted by Serine on average is shown in the Supporting Information in Section S4. In addition to $M1$, we can further ex-plore the conditional confusion matrix $P(Y|X)$ to inspect the probabilities of correct inference of each amino acid. For the case of optimized detector bands for 100 photons where $M1$ is 0.2449, we see that there is a higher probability of correctly inferring amino acids Serine, Phenylalanine and possibly Histidine and Leucine. Even these small numbers of correctly identified amino acids may be adequate to identify proteins from a database.[20,26] The optimization process outlined above could also be extended to optimize the posteriors of selected amino acids that would lead to higher protein identification accuracy.

2.2. Design of the SROE Filtering the Spectral Regions

The SROE will be placed in the focal plane of the last curved mirror of a spectrometer. Thus, all beams will hit the SROE perpendicular and parallel to each other. The general problem formulation is shown in **Figure 2a**. A single beam propagating along the z-direction hits the SROE from below at the position x. After the beam has propagated through the material with refractive index n, it reaches the top surface of the optical element which is described by the function $h(x)$. At this surface, the beam is refracted and further propagates under an angle α with respect to the z-axis. The refractive index of the air above the surface edge is assumed to be 1, so the refraction process is described by the local derivative of the height profile. Following the nomenclature from Figure 2a, from Snell's law for refraction at this surface we get $sin(\beta_2) = n \cdot sin(\beta_1)$. Here β_1 is the angle between the surface normal and the incident beam. This angle can directly be associated with the derivative of the height function $h'(x) = \tan(\beta_1)$. The angle β_2 describes the outcome angle with respect to the surface normal and can be expressed by $\beta_2 = \alpha + \beta_1$. The refracted beam propagates to the image plane which has the distance d to the entrance plane of the SROE and hits the image plane at
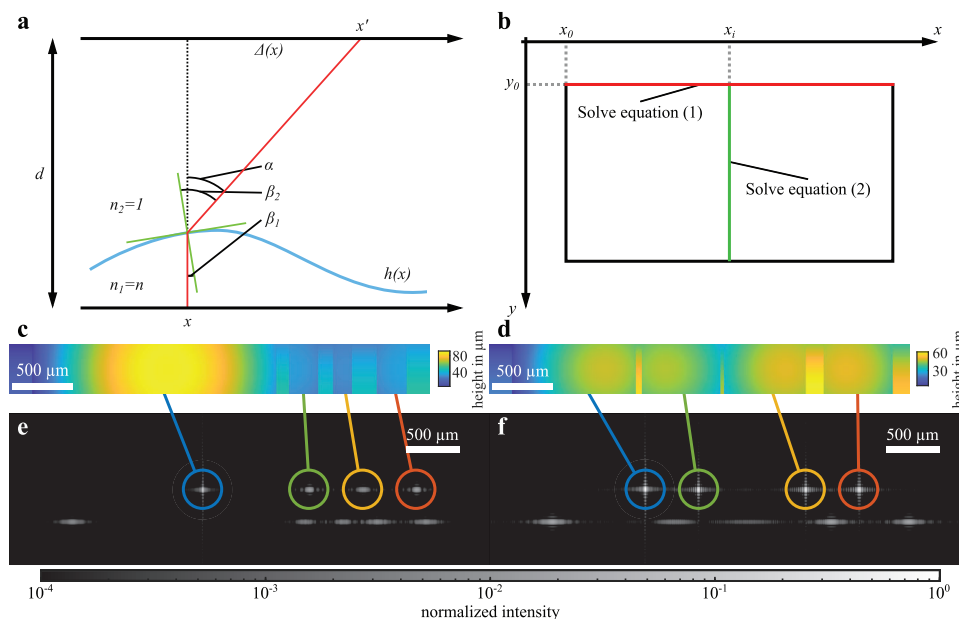
2401876 (3 of 7)

Figure 2. a) The SROE is an optical element guiding parallel incident beams at position x to position x'. The difference between these two positions can be expressed by a difference function $\Delta(x)$ which can again be expressed by geometrical boundaries to find a partial differential equation (PDE) for the height profile. b) This PDE can then be solved for the footprint area of the SROE in two dimensions solving it first along x-direction and then along y-direction. The solution for the given difference function is shown in (c,d), while (e,f) show wave-propagation simulations of these solutions. The found foci match the expected positions. By individual wave-propagation simulations with only parts of the height profile illuminated, it can also be proven that the spots stem from the correct regions.

position x'. This position will later be given by the desired design. Therefore, we introduce the difference function $\Delta(x) = x' - x$ which will be treated as given for now. It can be put into relations to the angles via $\Delta(x) = (d - h(x)) \cdot \tan(\alpha)$. Putting all this together, we find the following differential equation:

$$h'(x) = \frac{\Delta(x)}{n\sqrt{(d - h(x))^2 + \Delta(x)^2} - (d - h(x))} \qquad (5)$$

which can be generalized into a partial differential equation (PDE) for two dimensions by replacing x with (x, y) and transforming $\Delta(x)$ to a vector $\mathbf{\Delta}(x, y)$

$$\nabla h(x, y) = \frac{\mathbf{\Delta}(x, y)}{n\sqrt{(d - h(x, y))^2 + |\mathbf{\Delta}(x, y)|^2} - (d - h(x, y))} \qquad (6)$$

This generalization is justified by the fact that the refracted beam and the incident beam always lie in the same plane. For convenient notation, we introduce the auxiliary function

$$H(x, y, h) := \frac{1}{n\sqrt{(d - h)^2 + |\mathbf{\Delta}(x, y)|^2} - (d - h)} \qquad (7)$$

and split the PDE into two equations:

$$\partial_x h(x, y) = H(x, y, h) \cdot \Delta_x(x, y) \qquad (8)$$

$$\partial_y h(x, y) = H(x, y, h) \cdot \Delta_y(x, y) \qquad (9)$$

The solution strategy for these coupled PDEs is illustrated in Figure 2b. In one corner of the SROE's footprint the boundary condition has to be given by $h(x_0, y_0) = h_0$. From this corner one of the two equations can be solved along a line. Here, we chose to solve Equation (8) along x-direction, so we keep y_0 fixed as a constant (see red line in Figure 2b). Next, we can use the solution at each x-position x_i as a new starting value $h(x_i, y_0) = h_i$ to solve Equation (9) along y-direction. Thus, we can find a solution $h(x, y)$ for each point inside the rectangular region. Due to this strategy of solution, the height function h is only continuous along y-direction and along x-direction on the $y = y_0$ line. For $y \neq y_0$ the height function is not necessarily continuous along x-direction but it depends on the continuity of $\mathbf{\Delta}(x, y)$.

For the aimed application, the difference function $\mathbf{\Delta}(x, y)$ can be constructed in sections. Let I_i $(i = 1, \dots, 4)$ be the intervals in the spectral regions and x_i' $(i = 1, \dots, 4)$ the x-positions of the fiber endings. The spatial dependency of the wavelength $\lambda(x)$ along the x-direction in the spectrometer can be calculated using the focal length of the focusing mirror (300 mm), the grating used in the spectrometer (150 grooves/mm), and the excitation wavelength of 785 nm (see Supporting Information). The y-positions of the fiber endings are all set to 0. Therefore, we can say that the difference function for the intervals is given by $\mathbf{\Delta}(x, y) = (x_i' - x, -y)^T$ ($\forall x: \lambda(x) \in I_i$). In between the intervals the light should not be collected by the fibers. This is realized by refracting the light along y-direction, so it hits the image plane at $y_b' = 300$ μm displaced in y-direction. This number is a trade-off between a low height profile, which is easier to fabricate, and a large suppression of the

**ADVANCED
SCIENCE NEWS**

www.advancedsciencenews.com

**ADVANCED
MATERIALS
TECHNOLOGIES**

www.advmattechnol.de

light in between the intervals. So, the difference function in between the intervals can be written as $\mathbf{\Delta}(x, \gamma) = (0, \gamma_b{}' - \gamma)^T$ ($\forall x \forall i$: $\lambda(x) \notin I_i$).

The refractive index of the polymer is found to be 1.5053 at the center wavelength of 841.5 nm.[27] The distance between the SROE footprint plane and the fiber endings is chosen to be $d = 15$ mm. With these parameters together, the solution of the PDEs can be calculated. For the before demonstrated optimized bands the solutions are shown for 100 photons in average in Figure 2c, and for 50 photons in average in Figure 2d. To demonstrate the capabilities of the calculated structures a wave-propagation simulation was performed. The results are shown in Figure 2e,f respectively. By limiting the incident light to the spectral regions, one can show, that the four spots are indeed produced by the corresponding regions. The focus size is smaller than the core diameter of the optical fibers of about 440 µm. The light in between the intervals is refracted away from the positions of the fiber endings and, thus, filtered out.

3. Experimental Section

3.1. Fabrication of the SROE

The SROE was 3D printed with a Nanoscribe QuantumX exploiting the two-photon grayscale lithography (2GL) mode for 2.5D structures. This printing mode is especially suitable for optical-grade micro-optical components.[21] Under conditions closely similar to the ones used in the present paper, ref. [23] has reported an area-based mean roughness of 10 nm and a Root Mean Square (RMS) roughness of 13 nm.

The structure was printed using the medium-feature set consisting of a 25× objective lens as print head and the commercially available photoresist IP-S. The job file was generated in GrayScribeX version 4.0.1 and the machine ran with nanoSQX version 4.0.11. The printing parameters were left to the standard parameters suggested by Nanoscribe, i.e., a slicing distance of 1 µm, hatching distance of 200 nm, and a scan speed of 200 mm s⁻¹. The splitting period was chosen to be 420 µm, while the field overlap was 60 µm with activated 2GL stitching and a shear angle of 15°. The used 2GL profile was left to the generated profile by Nanoscribe, i.e., a minimum laser power of 8 mW, maximum laser power of 50 mW, and an exponent of 1.459. The multilayer attenuation was left to be 0.8.

After the exposure, the structure was developed in propylene glycol methyl ether acetate (PGMEA) for 20 minutes and later rinsed in isopropanol before putting it into another bath of isopropanol for 5 minutes. After the second bath, the structure was rinsed with fresh isopropanol again and dry blown with nitrogen to be ready for usage. An iterative precompensation scheme[22] with optical-confocal investigation did improve the surface precision, however, this did not have a significant impact on the optical performance (see Supporting Information).

3.2. Testing the SROE

Finally, it was demonstrated that the fabricated SROE indeed selects the correct spectral regions and couples them into the corresponding fibers. Therefore, we used a super-continuum white-light source (see spectrum in Supporting Information) split up

by a 300 grooves/mm optical grating (Thorlabs GR13-0310). The spectrum was focused by a curved mirror with a focal length of 150 mm (Thorlabs CM254-150-P01) onto the SROE's back plane. This combination of grating and curved mirror was equivalent to the configuration described in Section 2.2 as long as $\frac{1}{g^2} \gg \lambda_0^2$ (see Supporting Information). On the other hand, it profits from a shorter geometrical length on the optical table. In the image plane of the SROE, a camera was first put to observe the four foci. In **Figure 3a,b**, one can see the camera (IDS U3-3882LE-C) pictures from the two SROE versions for 100 photons on average and 50 photons on average, respectively. The intensity values in the images are normalized with respect to the highest pixel value. While in real Raman spectroscopy experiments a spectral sensitivity calibration would be applied, we have not done that here, possibly leading to small errors. However, the images agree very well with the simulations shown in Figure 2e,f. Next, the camera was replaced by a fiber stack consisting of 16 optical fibers with a core diameter of 440 µm and a core distance of 500 µm, for which the SROE was designed. The fiber stack could be aligned such that each focus was coupled into a fiber in parallel. No realignment was necessary for switching between the fibers. The light emerging from each fiber was analyzed by using a spectrometer (Ocean Insight FLAME-T-XR1-ES). The spectra are shown in Figure 3c,d, respectively. The optimized regions were shown as boxes in the background overlaid by the measured spectra as a curve. One can see that the widths and positions of the measured spectra match the boxes. Only for very small spectral regions, like the third one for the 100-photons-SROE illustrated in yellow in Figure 3c, the measured spectrum is wider than the design. This results from the limited resolution of the imaging system consisting of the curved mirror, which is not able to produce focus spots such small. For a beam diameter of 500 µm the spot size on the SROE's back plane is about 300 µm large, leading to a spectral resolution of about $\Delta\lambda = 6.5$ cm⁻¹, hence $\Delta\nu = 10.5$ cm⁻¹, while the smallest spectral region mentioned above is with a width of 3.5 nm a factor of 2 smaller. Therefore, light from neighboring wavelength regions is leaking in the focusing area. However, the position of the region still fits, and the device fulfills its job in that it couples the corresponding spectral region into the optical fiber.

Following this test, the SROE works fine for focusing given spectral regions into equidistant distributed optical fibers. In a spectroscopic experiment this means that the counts of the four detectors can be associated with photons stemming from the corresponding spectral regions – which was the target of the optimization. Therefore, this device/technique is crucial in boosting the performance of spectrometers based on few-element detectors with high yields.

4. Conclusion

Raman spectroscopy is a well-established means for the identification and sensing of molecules. However, when increasing the measurement speed, e.g., when rapidly sequencing proteins, the photon counts decrease and the reliable identification of molecules becomes an issue. Obviously, using high-quantum-efficiency photon detectors becomes crucial and one may want to use only a few of such (costly) detectors. When using only a few, a first conceptual challenge lies in identifying the positions
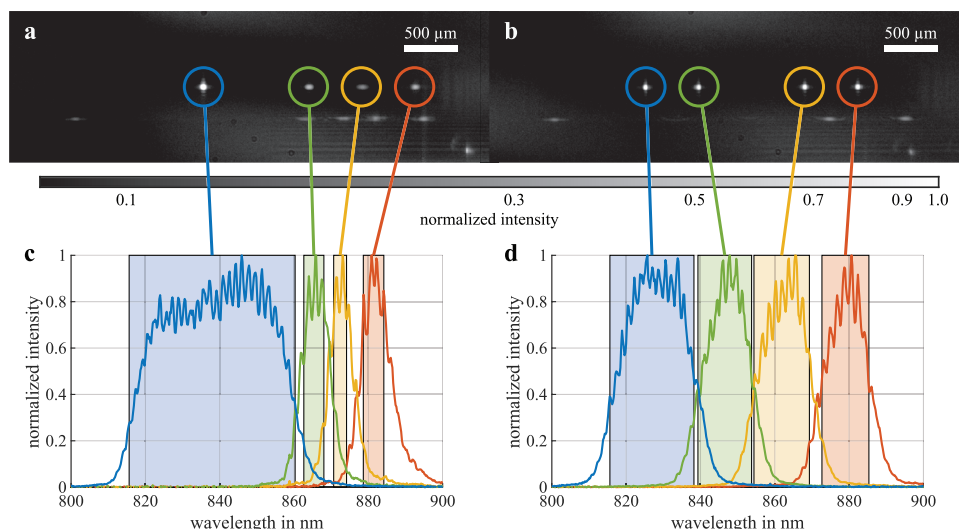
2401876 (5 of 7)

Figure 3. Test results of the two SROE versions: 100 photons on average on the left (a and c panels) and 50 photons on average on the right (b and d panels). The SROE is illuminated with a continuous spectrum in the given wavelength regime. In the image plane of the SROE, a camera is placed to observe the four foci (a and b) which match the images from the simulation. Next, we replace the camera by a fiber stack to couple the light from one focus into one optical fiber and measure the spectrum with a spectrometer. The measured spectra are shown as curves in c and d and match the calculated optimized regions illustrated as boxes in the background. The lines and circles indicate which spectrum was measured from which focus spot.

and widths of the corresponding few spectral regions. In the theoretical part of our study, we have found that the answer not only depends on the molecules to be identified but also on the anticipated average photon counts. Specifically, we have concentrated on the example of identifying proteins from the underlying 20 amino acids in a Raman spectrometer. A second challenge lies in the optics that distributes and focuses the light from generally unevenly wide and non-equidistantly spaced spectral regions with gaps in between onto evenly spaced small-area detectors or optical fibers connected to detectors. We have proposed a flexible and compact approach based on a segmented refractive-optical element. Herein, light within the selected spectral regions is focused off-axis onto the few detectors or fibers and the light within the spectral gaps is refracted out of the plane of incidence, allowing for efficient suppression. Samples with optically smooth surfaces have been manufactured by multi-photon 3D laser printing and successfully been tested in a spectrometer under conditions of white-light illumination. In the future, we plan to use such micro-optical elements in the framework of the European project ProID[28] for rapidly sequencing proteins using Raman signals.

All required experimental data can be accessed via the https://doi.org/10.35097/VLHKYhNypFOSgNdI.

Supporting Information

Supporting Information is available from the Wiley Online Library or from the author.

Acknowledgements

Conflict of Interest

The authors declare no conflict of interest.

Data Availability Statement

The data that support the findings of this study are openly available in Datenpaket: Distinction of low-intensity Raman spectra originating from amino-acids using a compact 3D printed micro-optical elements at https://doi.org/10.35097/VLHKYhNypFOSgNdI, reference number 35097.

Keywords

[1] D. Musumeci, C. Platella, C. Riccardi, F. Moccia, D. Montesarchio, *Cancers* **2017**, *9*, 174.

[2] C. Kretschmer, A. Sterner-Kock, F. Siedentopf, W. Schoenegg, P. M. Schlag, W. Kemmner, *Mol Cancer* **2011**, *10*, 15.

[3] N. Akkilic, S. Geschwindner, F. Höök, *Biosens. Bioelectron.* **2020**, *151*, 111944.

[4] P. Schanda, G. Haran, **2024**, *53*, 247.

[5] J. Martens, G. Berden, R. E. van Outersterp, L. A. J. Kluijtmans, U. F. Engelke, C. D. M. van Karnebeek, R. A. Wevers, J. Oomens, *Sci. Rep.* **2017**, *7*, 3363.

[6] F. Fan, Z. Feng, C. Li, *Chem. Soc. Rev.* **2010**, *39*, 4794.

[7] R. F. Kranenburg, F. A. M. G. van Geenen, G. Berden, J. Oomens, J. Martens, A. C. van Asten, *Anal. Chem.* **2020**, *92*, 7282.

[8] E. C. L. Ru, P. G. Etchegoin, *Annu. Rev. Phys. Chem.* **2012**, *63*, 65.

[9] G. Haran, *Acc. Chem. Res.* **2010**, *43*, 1135.

[10] Y. He, S. Su, T. Xu, Y. Zhong, J. A. Zapien, J. Li, C. Fan, S.-T. Lee, *Nano Today* **2011**, *6*, 122.

[11] Q. Ding, J. Wang, X. Chen, H. Liu, Q. Li, Y. Wang, S. Yang, *Nano Lett.* **2020**, *20*, 7304.

[12] J.-A. Huang, M. Z. Mousavi, Y. Zhao, A. Hubarevich, F. Omeis, G. Giovannini, M. Schütte, D. Garoli, F. De Angelis, *Nat. Commun.* **2019**, *10*, 5321.

[13] M. Iarossi, D. Darvill, A. Hubarevich, J.-A. Huang, Y. Zhao, A. F. De Fazio, D. B. O'Neill, F. Tantussi, F. De Angelis, *Adv. Funct. Mater.* **2023**, *33*, 2301934.

[14] Y. Zhao, A. Hubarevich, A. F. De Fazio, M. Iarossi, J.-A. Huang, F. De Angelis, *Nano Lett.* **2023**, *23*, 4830.

[15] Z. He, W. Qiu, M. E. Kizer, J. Wang, W. Chen, A. V. Sokolov, X. Wang, J. Hu, M. O. Scully, *ACS Photonics* **2021**, *8*, 424.

[16] Y. Zhao, M. Iarossi, A. F. De Fazio, J.-A. Huang, F. De Angelis, *ACS Photonics* **2022**, *9*, 730.

[17] N. Maccaferri, G. Barbillon, A. Nana Koya, G. Lu, G. P. Acuna, D. Garoli, *Nanoscale Adv.* **2021**, *3*, 633.

[18] W. Li, J. Zhou, N. Maccaferri, R. Krahne, K. Wang, D. Garoli, *Anal. Chem.* **2022**, *94*, 503.

[19] D. Garoli, H. Yamazaki, N. Maccaferri, M. Wanunu, *Nano Lett.* **2019**, *19*, 7553.

[20] B. K. Bhandari, N. Goldman, *NAR Genom. Bioinform.* **2024**, *6*, lqae126.

[21] S. Rodríguez, *PhotonicsViews* **2020**, *17*, 36.

[22] J. Weinacker, S. Kalt, P. Kiefer, P. Rietz, M. Wegener, *Adv. Funct. Mater.* **2024**, *34*, 2309356.

[23] T. Aderneuer, O. Fernández, R. Ferrini, *Opt. Express* **2021**, *29*, 39511.

[24] L. Siegle, S. Ristok, H. Giessen, *Opt. Express* **2023**, *31*, 4179.

[25] J.-A. Huang, M. Z. Mousavi, G. Giovannini, Y. Zhao, A. Hubarevich, M. A. Soler, W. Rocchia, D. Garoli, F. De Angelis, *Angew. Chem., Int. Ed. Engl.* **2020**, *59*, 11423.

[26] Y. Yao, M. Docter, J. van Ginkel, D. de Ridder, C. Joo, *Phys. Biol.* **2015**, *12*, 055003.

[27] IP-S-Tables, https://support.nanoscribe.com/hc/en-gb/articles/360009156133-IP-S-Tables, (accessed: June 2024).

[28] ProID, https://proidproject.eu/, (accessed: June 2024).